Magnetic Excitation and Thermodynamics of $BaFe_2As_2$

Y. WANG, S. L. SHANG, L. Q. CHEN, Z. K. LIU

Department of Materials Science and Engineering, The Pennsylvania State University, University Park, PA 16802

Received 13 May 2010; accepted 24 May 2010
Published online 26 October 2010 in Wiley Online Library (wileyonlinelibrary.wiley.com).
DOI 10.1002/qua.22865

ABSTRACT: Magnetic excitation of the iron-based superconductor parent compound $BaFe_2As_2$ at finite temperature are addressed with a first-principles formulation of the Helmholtz energy, which can account for the finite temperature mixture of many magnetic configurations. We find that it is the spin exchange coupling in the interplane *c* direction that dictates the spin density wave ordering. We have also quantitatively predicted the pressure dependence of the spin density wave ordering temperature, the Schottky anomaly, and the temperature dependence of thermal populations of several low-energy spin configurations, all in agreement with available experimental data. ©2010 Wiley Periodicals, Inc. Int J Quantum Chem 111: 3565–3570, 2011

Key words: pnictides; magnetic properties; heat capacity at magnetic critical points

Introduction

$BaFe_2As_2$ [1–3] is one of the most investigated parent compounds among the newly discovered iron arsenide superconductors [4] whose superconductive mechanism cannot be understood based on the BCS theory [5]. A variety of properties of $BaFe_2As_2$ have been measured, including the pressure effects [6, 7], the inelastic neutron scattering experiments for magnetic ordering and spin-density-wave (SDW) energy gap [8–14], Fermi surface [9], doping effects [2, 3, 8, 15, 16], electrical resistivity and susceptibility [17], and the phonon and thermodynamic properties [1, 2, 18]. There have also been many theoretical attempts to understand $BaFe_2As_2$, including that by Singh [19] within local-density approximation, that by Lorenzana et al. [20] under Hartree–Fock approximation and Landau theory, and that by Zbiri et al. [18] and that by Yildirim [21] for lattice dynamics without considering the thermodynamic or magnetic

Correspondence to: Y. Wang; e-mail: yuw3@psu.edu
Contract grant sponsor: Office of Naval Research (ONR).
Contract grant number: N0014-07-1-0638.
Contract grant sponsor: National Science Foundation (NSF).
Contract grant number: DMR-0510180.
Contract grant sponsor: DOE Basic Sciences.
Contract grant number: DOE DE-FG02-07ER46417.
Contract grant sponsor: Office of Science of the U.S. Department of Energy.
Contract grant number: DE-AC02-05CH11231.
Contract grant sponsor: Arctic Region Supercomputing Center at the University of Alaska Fairbanks as part of the Department of Defense High Performance Computing Modernization Program.

fluctuations. However, there has been lacking of thermodynamic formulation, which takes into account the magnetic excitations at finite temperatures. A clear distinction must be made here between the paramagnetic phase and the nonmagnetic phase. In the paramagnetic phase, Fe atoms possess local spin moments although disordered while in the nonmagnetic phase there are no local spin moments at Fe sites at all. In a series of works, an attempt has been made by us to develop a first-principles finite temperature thermodynamic framework [22, 23] for a system with itinerant magnetism. In this work, we show the application of our framework to $BaFe_2As_2$.

Definitions and Basic Formulas

We treat $BaFe_2As_2$ as a system at constant volume V and temperature T with itinerant collinear magnetism. Let us use N to represent the total number of atoms in the system and N_m to represent the number of lattice sites with local spin moments (or equivalently, magnetic moments) in the system. When we limit our consideration to the magnetic structures that are just distinguished by spin up and spin down distributions among the magnetic lattice sites, such a system will give rise to 2^{N_m} magnetic structures. Furthermore, let us use the term spin configuration σ to index those magnetic structures that are not equivalent each other by space group operations. According to our framework [22, 23], counting all possible spin (up and down) distributions among the magnetic lattice sites, the partition function of the system, Z, can be written as:

$$Z = \sum_{\sigma} w^{\sigma} Z^{\sigma} = \sum_{\sigma} w^{\sigma} \exp[-\beta F^{\sigma}(N, V, T)], \quad (1)$$

where $\beta = 1/k_B T$, w^{σ} is the multiplicity of the spin configuration σ, and $F^{\sigma}(N, V, T)$ is the Helmholtz free energy of the spin configuration σ. Note that we have completed the summation over all vibrational and electronic states confined to the spin configuration σ. This makes it immediately apparent that Z^{σ} is the partition function of the spin configuration σ, and $x^{\sigma} = w^{\sigma} Z^{\sigma}/Z$ is its thermal population. We note here that it is the multiplicity w^{σ} that mainly dictates the temperature dependence of x^{σ}. This can easily be understood by the fact that if we merge w^{σ} into the exponential part in Eq. (1), we will have an additional entropic contribution of $k_B T \ln w^{\sigma}$ to the free energy $F^{\sigma}(N, V, T)$. This entropic contribution linearly increases with temperature increase, leading to the changes in the relative thermodynamic stabilities of different spin configurations and thus magnetic phase transitions at a high temperature.

From Eq. (1), with $F = -k_B T \ln Z$ [24], we can find the total Helmholtz free energy of the system as

$$F(N, V, T) = \sum_{\sigma} x^{\sigma} F^{\sigma}(N, V, T) - T S_f(N, V, T), \quad (2)$$

where the configurational entropy is

$$S_f(N, V, T) = -k_B \sum_{\sigma} x^{\sigma} \ln(x^{\sigma}/w^{\sigma}). \quad (3)$$

We calculate $F^{\sigma}(N, V, T)$ using the following equation [22]

$$F^{\sigma}(N, V, T) = E_c^{\sigma}(N, V) + F_v^{\sigma}(N, V, T) + F_{\mathrm{el}}^{\sigma}(N, V, T), \quad (4)$$

where E_c^{σ} is the 0-K static total energy, F_v^{σ} the vibrational free energy, and F_{el}^{σ} the thermal electronic free energy.

We treat $BaFe_2As_2$ with an orthorhombic $a \times b \times 2c$ 40-atom supercell. Even considering only the collinear spin up and down flips of the 16 Fe atoms (i.e., $N_m = 16$), we get 65536 (2^{16}) magnetic structures. However, within the temperature range considered in this work, most of the 65,536 configurations can be ruled out due to their high energies. It has been seen from the literatures [25–29] that the low energy spin configurations must be the superstructures of that of the two-dimensional antiferromagnetic stripe phase [21] (Hereafter abbreviated as 2D-stripe) where within the *ab* plane a stripe-like Fe spin ordering pattern appears which breaks the four-fold rotational symmetry, whereas the nearest-neighbor Fe spins along the *c* axis are parallel [26]. For example, up to date the only other possible low energy configuration is that of "Checkerboard," which is higher than that the 2D-stripe configuration by 89 meV for a four chemical formula cell as calculated by Yildirim [21]. As a result, out of the 65536 configurations, only 13 low-energy spin configurations are derived from the 40-atom supercell. Together with their multiplicities, the 13 spin configurations account for 256 spin up and spin down distributions.

For the convenience of discussions below, the 13 derived spin configurations are labeled as

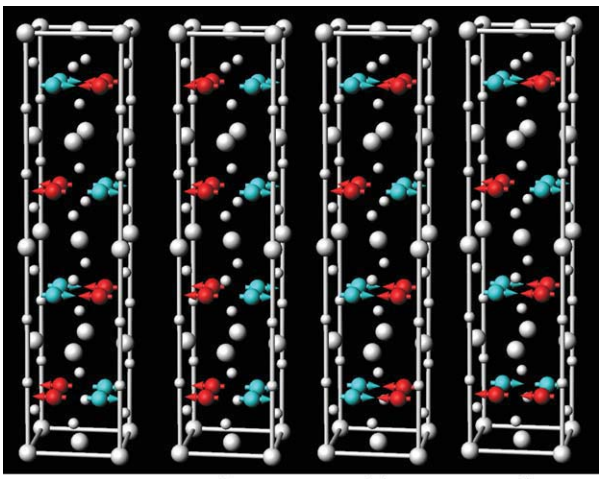

FIGURE 1. Selected spin configurations of $BaFe_2As_2$ with (a) SDW-AFM; (b) 2D-stripe; (c) STR6398; and (d) STR6980. Big grey balls: Ba; Small grey balls: As; Red balls with arrows pointing left: Fe with spin up; Cyan balls with arrows pointing right: Fe with spin down. [Color figure can be viewed in the online issue, which is available at wileyonlinelibrary.com.]

SDW-AFM, STR6398, STR6433, STR6980, STR6993, STR6425, STR7000, STR6978, STR17, STR6415, 2D-stripe, STR6396, and STR6406 (their w^σ as defined in Eq. (1) are 4, 16, 8, 32, 16, 64, 8, 16, 8, 32, 4, 32, and 16, respectively). The spin configurations of SDW-AFM, 2D-stripe, STR6398, and STR6980 are illustrated in Figure 1. The SDW-AFM configuration in Figure 1(a) is the experimentally determined ground state [30, 31] of $BaFe_2As_2$. Within the *ab* plane the Fe spins in the SDW-AFM configuration form the same magnetic configurations as that of 2D-stripe, whereas the nearest-neighbor Fe spins along the *c* axis are antiparallel, in contrast to that of 2D-stripe configuration in Figure 1(b). STR6398 [Fig. 1(c)] and STR6980 [Fig. 1(d)] represent two new excited spin configurations, relative to the SDW-AFM configuration.

Numerical Results and Discussion

To calculate the 0 K energies, we use the projector-augmented wave (PAW) method [32, 33] within the generalized gradient approximation (GGA) of Perdew–Burke–Ernzerhof (PBE) [34] as implemented in the VASP package [32, 33]. A plane wave cutoff of 348.2479 eV and a $6 \times 6 \times 4$ Γ-centered *k*-point mesh are used. The energies are converged to 10^{-6} eV. Total energies are calculated at 10 different volumes by a volume step of 4.5%. At each volume, both the cell shape and internal atomic positions are relaxed. At any arbitrary volume, Morse function [35, 36] is used to interpolate and smoothen the 0-K total energy curves. For the lattice vibration, we find that the Debye-Grüneisen approach [35, 36] is fast and yet sufficiently accurate for the present problem, considering that the SDW ordering is mainly dictated by the multiplicities w^σ as discussed with Eq. (1). The calculation of F^σ_{el} in Eq. (4) follows the previous work [22, 37, 38].

Figure 2 presents the first-principles 0 K total energies of the 13 spin configurations as a function of volume. For the SDW-AFM configuration, the calculated equilibrium lattice parameters, arsenic internal coordinate, and supercell volume are 5.70450 Å, 5.61533 Å, 12.8897 Å, 0.35028, and 825.781 Å^3, which are in close agreement with measured values of 5.61587 Å, 5.57125 Å, 12.9428 Å, 0.35406, and 809.894 Å^3 of the orthorhombic phase at 5 K by Huang et al. [10]. The calculated volume is larger than the measured one by 2%, which is typically acceptable considering the overall overestimation of volume by the GGA functional [39]. The calculated supercell equilibrium volumes for the other 12 spin configurations are ~1 Å^3 within that of the SDW-AFM configuration.

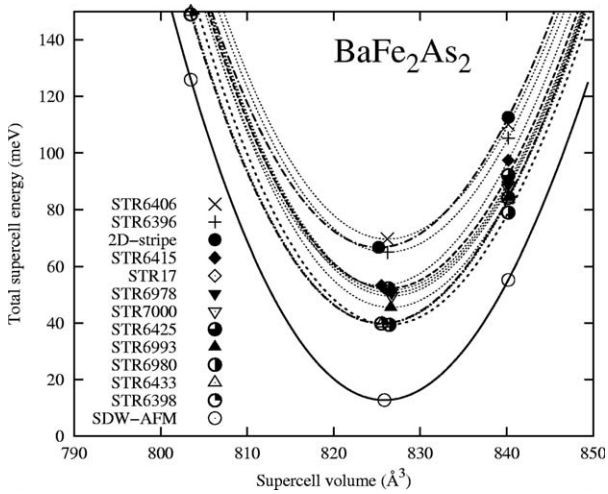

FIGURE 2. Calculated supercell energies of $BaFe_2As_2$ as a function of the $a \times b \times 2c$ 40-atom supercell volume. The symbols represent the calculated points and the lines represent the smoothened interpolation using Morse function.

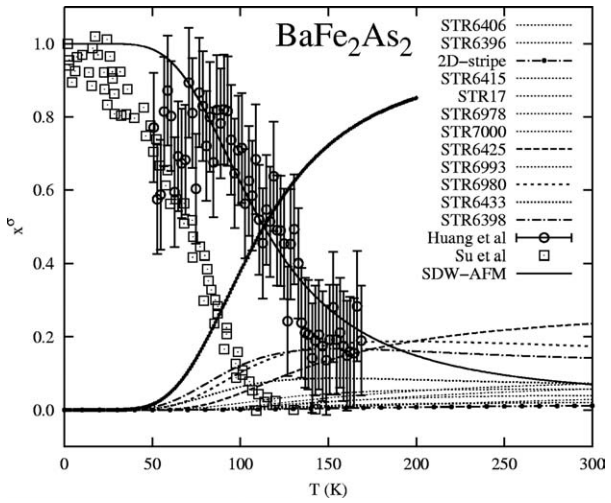

FIGURE 3. Thermal populations of the 13 spin configurations of $BaFe_2As_2$ as a function of temperature. The lines represent the calculations. The heavy black line represents the summation (only up to 200 K for the clarity of the plot) of the thermal population of all spin configurations except that of SDW-AFM. The circles with error bars are the measured (1, 0, 3) magnetic peak intensity of the SDW-AFM configuration by Huang et al. [10]. The squares are the measured (1, 0, 3) magnetic peak intensity of the SDW-AFM configuration by Su et al. [14].

It is seen from Figure 2 that the ground state is SDW-AFM, in agreement with existing measurements [30, 31]. We find that the first excited state is STR6398 with ~26.4 meV higher than the ground state. We note that the spin configuration STR6398 [see Fig. 1(c)] is the result of the simultaneous spin flipping of one of the four Fe layers of that of SDW-AFM in *c* direction. STR6398 cannot be expressed by a single commensurate spin wave state. Therefore, it is not surprising that the calculated excitation energy of ~26.4 meV from SDW-AFM to STR6398 is different from the observed SDW excitation gap of ~10 meV [8, 9, 12, 40], which might be the result of long range interaction, which cannot be considered in the present work. It is further seen that from Figure 2 the energies of most of spin configurations studied in this work are lower than that of the 2D-stripe configuration. In fact, Figure 3 shows that the thermal population of the 2D-stripe configuration is rather small. This somewhat raises a doubt about all the existing theoretical models based on the 2D-stripe configuration. Therefore, the magnetism in $BaFe_2As_2$ is more appropriately categorized as anisotropic three-dimensional as that found in $CaFe_2As_2$ [41] and in $SrFe_2As_2$ [42]. This is in disagreement with the measurements of anisotropy of resistivity and susceptibility in high-quality single crystal by Wang et al. [17] who show that $BaFe_2As_2$ is quasi-two-dimensional. However, the recent laser angle-resolved photoemission spectroscopy (ARPES) measurement by Shimojima et al. [43] suggests that Fermi surface of $BaFe_2As_2$ is highly three-dimensional in antiferromagnetic state. In addition, the measured anisotropies of electrical resistivity, upper critical field, London penetration depth, and critical currents of slightly Cobalt doped $BaFe_2As_2$ by Tanatar et al. [44] show that iron pnictide superconductors manifest anisotropies consistent with essentially three-dimensional intermetallic compounds. Furthermore, the ground state magnetic configuration of $BaFe_2As_2$ is undoubtedly three-dimensional [8, 14], indicating that two-dimensional models cannot accurately describe it.

Figure 3 depicts calculated thermal populations (x^σ) of the 13 spin configurations as a function of temperature. For comparison, the experimentally measured (1, 0, 3) magnetic peak intensity [10, 14] of the SDW-AFM configuration as a function of temperature is also shown. Our theory predicts very well the measured data by Huang et al. [10]. From Figure 3, it is seen that the thermal population of the SDW-AFM configuration decreases fast above 50 K. This indicates the start of magnetic phase transitions.

From Eq. (3), the magnetic specific heat because of the thermodynamic fluctuations among many magnetic configurations can be derived as [23, 24]

$$C_m = \frac{1}{k_B T^2}\left\{\sum_\sigma x^\sigma (E^\sigma)^2 - \left[\sum_\sigma x^\sigma E^\sigma\right]^2\right\}, \quad (5)$$

with the internal energy given by $E^\sigma = F^\sigma + TS^\sigma$ and the entropy of spin configuration σ given by $S^\sigma = -(\partial F^\sigma/\partial T)_V$. Eq. (5) is a generalization of the Schottky specific heat anomaly for a two-state system [24]. Figure 4 shows our predicted temperature evolution of the magnetic specific heat. For comparison, we also plot the measured magnetic specific heat that we have extracted from the measured total specific heat by Ni et al. [2] and the lattice specific heat by Mittal et al. [1] using the lattice dynamics approach in fitting the measured phonon density-of-states. We clearly see a peak along the magnetic specific heat curve at

~100 K, which demonstrates a Schottky anomaly, which is within the measured SDW ordering temperatures of 80–150 K [1–3, 10, 14]. It should be noted that the 40-atom supercell used here is not large enough to fully account for the long range interactions, such as those among magnetic dipoles.

Figure 5 shows the calculated SDW ordering temperature (T_{SDW}) as a function of pressure. The theoretical T_{SDW} is selected when the thermal population of the SDW-AFM spin configuration is decreased to 50%. In comparison, the measured T_{SDW} by Fukazawa et al. [7] are also plotted in Figure 5. The characteristic temperature T^* is evaluated at the thermal population of the SDW-AFM spin configuration equal to 99.99%. Both show remarkable agreement with experimental data.

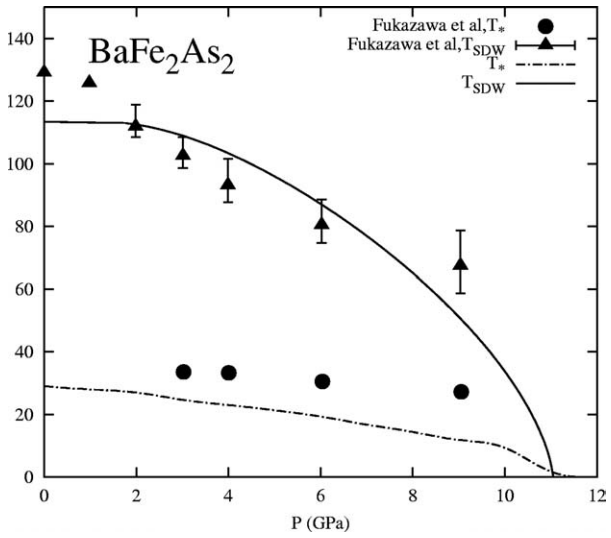

FIGURE 5. SDW ordering of $BaFe_2As_2$. The calculated ordering temperature T_{SDW} and the characteristic temperature T^* are shown by solid line and dot-dashed line, respectively. The measured T_{SDW} and T^* by Fukazawa et al. [7] are shown by triangles with error bars and circles, respectively.

Conclusions

In summary, we studied the magnetic excitation of the iron-based superconductor parent compound $BaFe_2As_2$ with addressing the finite temperature mixture of many spin configurations using our recently developed approach for a system with itinerant magnetism. Treating $BaFe_2As_2$ with an orthorhombic $a \times b \times 2c$ 40-atom supercell, we have calculated the energies of 13 low energies spin configurations, which account for 256 spin up and spin down distributions. Under the framework of itinerant collinear magnetism, it is found that the energies of most of spin configurations studied in this work are lower than that of the widely used 2D-stripe configuration in the literatures, which means that the spin exchange coupling in the interplane c direction dictates the spin density wave ordering. Furthermore, with a first principles formulation of the Helmholtz energy, which can account for the finite temperature mixture of many magnetic configurations, we have quantitatively predicted the pressure dependence of the spin density wave ordering temperature, the Schottky anomaly along the heat capacity curve, which is within the measured SDW ordering temperatures of 80–150 K, and the temperature dependence of thermal populations of the 13 spin configurations, all in agreement with available experimental data. Our approach is applicable to many other highly correlated magnetic systems.

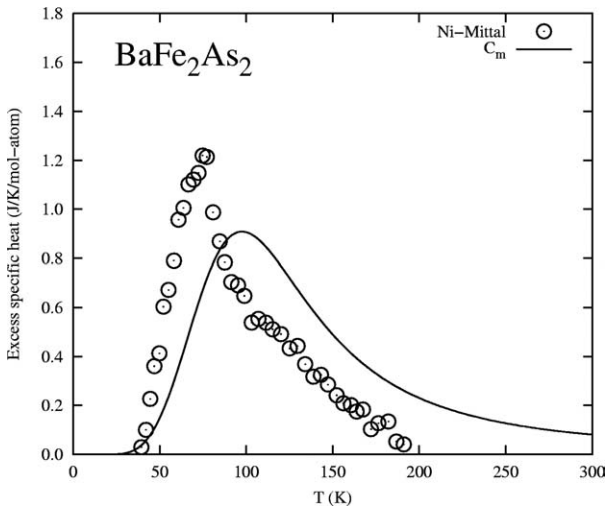

FIGURE 4. Magnetic specific heat (C_m) of $BaFe_2As_2$. The line illustrates the calculated value. The open circles are the measured magnetic specific heat that we extracted from the measured total specific heat by Ni et al. [2] and the lattice specific heat by Mittal et al. [1] using the lattice dynamics approach in fitting the measured phonon density-of-states.

ACKNOWLEDGMENTS

Calculations were conducted at the LION clusters at the Pennsylvania State University and at the National Energy Research Scientific Computing Center. The authors are indebted to Dr.

R. Mittal for sending us the heat capacity data. Communications with Dr. N. Ni and Dr. W. Hermes are acknowledged.

References

1. Mittal, R.; Su, Y.; Rols, S.; Chatterji, T.; Chaplot, S. L.; Schober, H.; Rotter, M.; Johrendt, D.; Brueckel, T. Phys Rev B 2008, 78, 104514.
2. Ni, N.; Bud'ko, S. L.; Kreyssig, A.; Nandi, S.; Rustan, G. E.; Goldman, A. I.; Gupta, S.; Corbett, J. D.; Kracher, A.; Canfield, P. C. Phys Rev B 2008, 78, 014507.
3. Rotter, M.; Tegel, M.; Johrendt, D. Phys Rev Lett 2008, 101, 107006.
4. Kamihara, Y.; Watanabe, T.; Hirano, M.; Hosono, H. J Am Chem Soc 2008, 130, 3296.
5. Bardeen, J.; Cooper, L. N.; Schrieffer, J. R. Phys Rev 1957, 108, 1175.
6. Ahilan, K.; Balasubramaniam, J.; Ning, F. L.; Imai, T.; Sefat, A. S.; Jin, R.; McGguire, M. A.; Sales, B. C.; Mandrus, D. J Phys-Condes Matter 2008, 20, 472201.
7. Fukazawa, H.; Takeshita, N.; Yamazaki, T.; Kondo, K.; Hirayama, K.; Kohori, Y.; Miyazawa, K.; Kito, H.; Eisaki, H.; Iyo, A. J Phys Soc Jpn 2008, 77, 105004.
8. Christianson, A. D.; Goremychkin, E. A.; Osborn, R.; Rosenkranz, S.; Lumsden, M. D.; Malliakas, C. D.; Todorov, I. S.; Claus, H.; Chung, D. Y.; Kanatzidis, M. G.; Bewley, R. I.; Guidi, T. Nature 2008, 456, 930.
9. Ding, H.; Richard, P.; Nakayama, K.; Sugawara, K.; Arakane, T.; Sekiba, Y.; Takayama, A.; Souma, S.; Sato, T.; Takahashi, T.; Wang, Z.; Dai, X.; Fang, Z.; Chen, G. F.; Luo, J. L.; Wang, N. L. EPL 2008, 83, 47001.
10. Huang, Q.; Qiu, Y.; Bao, W.; Green, M. A.; Lynn, J. W.; Gasparovic, Y. C.; Wu, T.; Wu, G.; Chen, X. H. Phys Rev Lett 2008, 101, 257003.
11. Rotter, M.; Tegel, M.; Johrendt, D.; Schellenberg, I.; Hermes, W.; Pottgen, R. Phys Rev B 2008, 78, 020503.
12. Matan, K.; Morinaga, R.; Iida, K.; Sato, T. J. Phys Rev B 2009, 79, 054526.
13. Pfuner, F.; Analytis, J. G.; Chu, J. H.; Fisher, I. R.; Degiorgi, L. Eur Phys J B 2009, 67, 513.
14. Su, Y.; Link, P.; Schneidewind, A.; Wolf, T.; Adelmann, P.; Xiao, Y.; Meven, M.; Mittal, R.; Rotter, M.; Johrendt, D.; Brueckel, T.; Loewenhaupt, M. Phys Rev B 2009, 79, 064504.
15. Liu, C.; Samolyuk, G. D.; Lee, Y.; Ni, N.; Kondo, T.; Santander-Syro, A. F.; Bud'ko, S. L.; McChesney, J. L.; Rotenberg, E.; Valla, T.; Fedorov, A. V.; Canfield, P. C.; Harmon, B. N.; Kaminski, A. Phys Rev Lett 2008, 101, 177005.
16. Sefat, A. S.; Jin, R. Y.; McGuire, M. A.; Sales, B. C.; Singh, D. J.; Mandrus, D. Phys Rev Lett 2008, 101, 117004.
17. Wang, X. F.; Wu, T.; Wu, G.; Chen, H.; Xie, Y. L.; Ying, J. J.; Yan, Y. J.; Liu, R. H.; Chen, X. H. Phys Rev Lett 2009, 102, 117005.
18. Zbiri, M.; Schober, H.; Johnson, M. R.; Rols, S.; Mittal, R.; Su, Y. X.; Rotter, M.; Johrendt, D. Phys Rev B 2009, 79, 064511.
19. Singh, D. J. Phys Rev B 2008, 78, 094511.
20. Lorenzana, J.; Seibold, G.; Ortix, C.; Grilli, M. Phys Rev Lett 2008, 101, 186402.
21. Yildirim, T. arXiv:0902.3462v1 [cond-mat.supr-con], 2009.
22. Wang, Y.; Hector, L. G.; Zhang, H.; Shang, S. L.; Chen, L. Q.; Liu, Z. K. Phys Rev B 2008, 78, 104113.
23. Wang, Y.; Hector, L. G.; Zhang, H.; Shang, S. L.; Chen, L. Q.; Liu, Z. K. J Phys-Condes Matter 2009, 21, 326003.
24. Kittel, C. Introduction to solid state physics; 8th ed.; Wiley: Hoboken, NJ, 2005.
25. Akturk, E.; Ciraci, S. Phys Rev B 2009, 79, 184523.
26. Dong, J.; Zhang, H. J.; Xu, G.; Li, Z.; Li, G.; Hu, W. Z.; Wu, D.; Chen, G. F.; Dai, X.; Luo, J. L.; Fang, Z.; Wang, N. L. EPL 2008, 83, 27006.
27. Mazin, II; Johannes, M. D.; Boeri, L.; Koepernik, K.; Singh, D. J. Phys Rev B 2008, 78, 085104.
28. Si, Q. M.; Abrahams, E. Phys Rev Lett 2008, 101, 076401.
29. Yin, Z. P.; Lebegue, S.; Han, M. J.; Neal, B. P.; Savrasov, S. Y.; Pickett, W. E. Phys Rev Lett 2008, 101, 047001.
30. de la Cruz, C.; Huang, Q.; Lynn, J. W.; Li, J. Y.; Ratcliff, W.; Zarestky, J. L.; Mook, H. A.; Chen, G. F.; Luo, J. L.; Wang, N. L.; Dai, P. C. Nature 2008, 453, 899.
31. Ewings, R. A.; Perring, T. G.; Bewley, R. I.; Guidi, T.; Pitcher, M. J.; Parker, D. R.; Clarke, S. J.; Boothroyd, A. T. Phys Rev B 2008, 78, 220501.
32. Blöchl, P. E. Phys Rev B 1994, 50, 17953.
33. Kresse, G.; Joubert, D. Phys Rev B 1999, 59, 1758.
34. Perdew, J. P.; Burke, K.; Ernzerhof, M. Phys Rev Lett 1996, 77, 3865.
35. Moruzzi, V. L.; Janak, J. F.; Schwarz, K. Phys Rev B 1988, 37, 790.
36. Wang, Y.; Ahuja, R.; Johansson, B. Int J Quant Chem 2004, 96, 501.
37. Jarlborg, T.; Moroni, E. G.; Grimvall, G. Phys Rev B 1997, 55, 1288.
38. Wang, Y. Phys Rev B 2000, 61, 11863.
39. Wang, Y.; Curtarolo, S.; Jiang, C.; Arroyave, R.; Wang, T.; Ceder, G.; Chen, L. Q.; Liu, Z. K. CALPHAD 2004, 28, 79.
40. Chi, S. X.; Schneidewind, A.; Zhao, J.; Harriger, L. W.; Li, L. J.; Luo, Y. K.; Cao, G. H.; Xu, Z. A.; Loewenhaupt, M.; Hu, J. P.; Dai, P. C. Phys Rev Lett 2009, 102, 107006.
41. McQueeney, R. J.; Diallo, S. O.; Antropov, V. P.; Samolyuk, G. D.; Broholm, C.; Ni, N.; Nandi, S.; Yethiraj, M.; Zarestky, J. L.; Pulikkotil, J. J.; Kreyssig, A.; Lumsden, M. D.; Harmon, B. N.; Canfield, P. C.; Goldman, A. I. Phys Rev Lett 2008, 101, 227205.
42. Zhao, J.; Ratcliff, W.; Lynn, J. W.; Chen, G. F.; Luo, J. L.; Wang, N. L.; Hu, J. P.; Dai, P. C. Phys Rev B 2008, 78, 140504.
43. Shimojima, T.; Ishizaka, K.; Ishida, Y.; Katayama, N.; Ohgushi, K.; Kiss, T.; Okawa, M.; Togashi, T.; Wang, X.-Y.; Chen, C.-T.; Watanabe, S.; Kadota, R.; Oguchi, T.; Chainani, A.; Shin, S. Phys Rev Lett 2010, 104, 057102.
44. Tanatar, M. A.; Ni, N.; Martin, C.; Gordon, R. T.; Kim, H.; Kogan, V. G.; Samolyuk, G. D.; Bud'ko, S. L.; Canfield, P. C.; Prozorov, R. Phys Rev B 2009, 79, 094507.